DEEP LEARNING POWERED HYBRID FRAMEWORK FOR MULTICLASS HISTOPATHOLOGY BASED CANCER DIAGNOSIS

PRIYANKA KHABIYA[1], PROF(DR.)FIROJ PARWEJ[2]

[1]Research Scholar, MANDSAUR UNIVERSITY, Department of CSE, Mandsaur,India

[2]Professor, MANDSAUR UNIVERSITY, Department of CSE, Mandsaur,India

E-mail: [1]priyanka.khabiya@meu.edu.in, [2]firoj.parwej@meu.edu.in

ABSTRACT

This work introduces an explainable deep learning approach for classifying lung and colon cancer using histopathological images. Recent improvements in deep learning have significantly enhanced medical image analysis; however, most existing models still suffer from poor interpretability, limited transparency, and weak generalization across tissue types. To address these gaps and enhance clinical trust, this study proposes a transparent and reliable deep learning framework for cancer diagnosis. The framework influences a custom Convolutional Neural Network architecture, enhanced by the Swish activation function to enhance merging and representation learning. This architectural selection enables better feature extraction and convergence compared to traditional activation functions, resulting in an improved overview across histopathological patterns. To improve transparency and model responsibility, explainability techniques, such as Gradient-weighted Class Activation Mapping (Grad-CAM) and Integrated Gradients (IG), are employed, providing visual insights into the regions that contribute to model predictions. Evaluated on a standard histopathology dataset, the proposed model achieves high classification performance with 98.69% accuracy, 98.71% precision, 98.69% recall, and 98.70% F1-Score. The visual attribution maps confirm that the network attends to the diagnostically major tissue regions, reinforcing its reliability in medical image analysis. The significant impact of this study is that it demonstrates the potential of combining an optimized CNN architecture with explainable AI methods to improve diagnostic accuracy and interpretability concurrently. The findings propose that combining advanced CNN design with an explainability technique can bring both accuracy and interpretability in digital pathology applications.

Keywords: *Deep Learning, Histopathology, Lung Cancer, Colon Cancer, SegNet, EfficientNet, VGG16, Explainable AI, Grad-CAM, Integrated Gradients*

1. INTRODUCTION

Cancer remains a leading cause of death worldwide, with lung and colon cancers accounting for a significant portion of cancer-linked deaths and disease[10].This method focuses especially on histopathological image-based analysis of lung and colon cancer by using digital H&E-stained slides.It does not include other modalities such as CT, MRI, or genomic data, ensuring a clear and focused research scope. The prognosis for these malignancies suggests that it improves when detected at an early stage, emphasizing the importance of a suitable and accurate diagnosis. Traditional investigative techniques, such as histopathological assessment under the microscope and CT imaging analysis, although widely used, are often labor-intensive, time-consuming, and dependent on individual clinical expert interpretation [4], [5]. These limits have advised an example shift toward automated analytical systems, with deep learning methods emerging as promising solutions due to their ability to deliver high accuracy, efficiency, and reproducibility [2],[6],[15]. Within the domain of histopathological image analysis, convolutional neural networks have gained significance due to their ability to extract complex spatial and morphological patterns from tissue slides. These models have been efficiently utilized for jobs such as tumor localization [4], cancer subtype classification [10], and cellular structure analysis [5], [13]. Notable architectures, including ResNet [12], EfficientNet [20], and attention-based U-Net models [11], [25] have established outstanding results when applied to Hematoxylin and Eosin (H&E) stained histology images. Furthermore, area expert networks, such as

LymphoNet [6] and HistoNeXt [10], have introduced architectural innovations to better accommodate tissue variability and high-dimensional image features commonly observed in medical imaging.Even with these improvements, most current models still lack interpretability and transparency.Few studies have attempted to integrate optimized activation functions with explainable AI to enhance model reliability and clinical trust.Similarly, segmentation networks such as U-Net and its variants have been used to delineate regions of interest, providing valuable support for clinical assessment and contributing to the interpretability of predictions [11], [22]. To further improve model transparency, techniques similar to Gradient weighted Class Activation Mapping and SHAP have been incorporated into CNN pipelines, enabling visual details of decision margins, a critical prerequisite for clinical adoption [31], [34]. Hence, there is a persistent need for frameworks that not only attain high diagnostic correctness but also clarify their decision-making process.This interpretability is vital for fostering medical assurance and promoting the real-world acceptance of AI-assisted verdicts.Transfer learning and ensemble methods are also commonly employed to moderate the challenge of limited annotated data, allowing for efficient variation of pretrained models, such as VGG, EfficientNet, and ResNet [28], [30], [31].Substantial progress has also been observed in CT-based diagnostic systems for lung cancer, where hybrid pipelines merging segmentation and classification stages have established efficiency in classifying lung nodules and malignancies [32], [33].However, numerous existing systems operate as black boxes, failing to provide visual validation for their output.This raises the research question: Can an enhanced CNN framework, combined with explainable AI methods, achieve high accuracy and interpretability for lung and colon cancer classification? Advanced strategies such as domain adaptation and weak supervision have been introduced to advance generalization in heterogeneous datasets and decrease dependency on extensive annotations [13], [18].Even though these advancements exist, key obstacles remain, including class imbalance, model interpretability, annotation scarcity, and poor generalization across diverse datasets. Modern innovations intend to address these issues through a generative approach, such as GAN-based data augmentation [27], self-supervised learning [13], and virtual staining technique using generative models [17], [19], which improve both data diversity and model robustness. Numerous studies have established the potential of DL models utilizing CNNs, transfer learning, attention mechanisms, and a hybrid ensemble strategy in enhancing the accuracy, interpretability, and reliability of cancer diagnosis in both histopathology and CT imaging domains.This research proposes a hybrid deep learning framework that incorporates a Swish-activated CNN architecture for classifying lung and colon histopathological images of cancer. This study is limited to publicly accessible histopathology datasets and adopts accurate labeling and reliable staining excellence.It does not discuss clinical arrangements, real-time processing, or multimodal data fusion with radiology images.These model decisions are interpreted using GradCAM and Integrated Gradients, ensuring visual transparency.The primary goal of this study is to propose a transparent deep learning framework that strikes a balance between diagnostic accuracy and interpretability.Its novelty lies in combining a Swish-activated CNN with explainability tools, such as Grad-CAM and Integrated Gradients, to bridge the gap between accuracy and trustworthiness. The framework achieves high classification performance, with an accuracy of 98.69%, a precision of 98.71%, a recall of 98.69%, and an F1 Score of 98.70%, indicating its potential as a reliable tool for medical image analysis.

2. RELATED WORK

2.1 Histopathology-Based Deep Learning Methods

Hiran and Yadav [1] developed an ensemble model for colon cancer identification by combining ResNet and VGG architectures. Their understanding achieved an accuracy of 94.6%, precision of 92.1%, and recall of 93.3% on the TCGA dataset. This fusion approach addresses feature redundancy and better classification robustness. Lu et al. [2] developed a scalable deep learning (Dl) based segmentation framework for whole-slide images, leveraging a U-Net variant trained with custom-made loss functions. Their categorization enabled pixel-wise tumor delineation with a Dice coefficient of 0.89 on CAMELYON16 and a high outcome for clinical settings. Spanhol et al. [3] contributed a breast cancer dataset and evaluated the performance of CNN on it. Their research with LeNet and AlexNet variants presented baseline accuracies ranging from 84% to 91%, depending on image magnification and preprocessing strategies. Zhou and Wang [5] presented a CNN framework for hepatic ploidy analysis from H&E images, reporting 90.4% accuracy and 89.3% precision, with

ISSN: 1992-8645 www.jatit.org E-ISSN: 1817-3195

applicability to liver cancer progression monitoring. LymphoNet, presented by Talo et al. [6], focuses on classifying lymph node histopathology images using a custom CNN with enhanced filters. It reached

Achieving 96.3% accuracy, 94.7% precision, and 95.4% recall, our method significantly outperforms traditional feature-based methods. Patel and Mehta [7] provided a comprehensive review of deep and transfer learning applications in histopathology, identifying hybrid CNN-Transformer models as emerging techniques with accuracies exceeding 95% in certain breast and colon cancer datasets. Mobadersany et al. [8] merged histology and genomic data using CNNs for prognostic classification. Their combined system achieved a c-index of 0.77, improving outcome prediction over purely histological models. Pan et al. [9] established a lightweight model called SDENet for breast cancer histopathological classification. Their construction reduced computational overhead while attaining 93.1% accuracy and an F1-score of 0.91. Khan et al. [10] presented HistoNeXt, a DL-based model considered for colon cancer classification. Constructed upon a residual attention mechanism, it upgraded feature localization. The model attained 95.2% accuracy and a recall of 94.3% using a curated histopathology dataset. Sharma and Desai [11] proposed a hybrid U-Net model combined with attention gates for lung cancer cell segmentation. The system achieves a Dice score of 0.87 and a precision of 89.1%, indicating a strong performance in cellular boundary delineation on H&E-stained images. Śmieja and Nowak [12] recognized the combination of ResNet50 with attention modules for histopathology classification. The model achieved 93.6% accuracy and a precision of 91.5%, along with a recall of 92.4%, indicating a better focus on discriminative tissue regions. Wu et al. [13] anticipated a weakly supervised, self-supervised learning method that incorporates mutual region attention for sparse label settings. Their model achieves 92.5% accuracy and considerably reduced training time, illustrating its potential in data-controlled scenarios.

2.2 CT-Based Cancer Diagnosis Using Deep Learning

Ounkomol et al. [17] and Hoffer et al. [19] presented deep learning-based virtual staining methods that generate synthetic H&E images from label-free tissue, thereby reducing dependency on chemical staining while maintaining classification accuracy above 90%. He et al. [18] introduce a domain-invariant transfer learning technique to mitigate distributional shifts across institutions. The method reported a relative 5.2% development in cross-center colon cancer classification. Mahapatra et al. [27] employed a GAN-based image improvement technique to simulate unpaired domain translations in histopathology images, resulting in a 4% improvement in classification accuracy in low-resolution domains. Aha et al. [28] proposed VERNet, a hybrid ensemble that integrates VGG19, EfficientNetB0, and ResNet101 for lung cancer detection. The model accomplished 91.3% accuracy, 90.7% precision, and 91.2% recall on a curated CT dataset, demonstrating strength through architecture fusion.LungEffNet [29], a classifier built on EfficientNet-B3, was considered for lung cancer detection from CT scans. It outperformed previous CNN models, achieving 96.1% accuracy, 95.8% precision, and 94.9% recall, thanks to compound scaling techniques. Wang et al. [30] implemented a deep hybrid pipeline that merges EfficientNet-B3 and custom classifiers for multiclass CT diagnosis. Their model achieved 98.3% accuracy, with F1 scores of 0.95 across classes, including benign and malignant types. Divya et al. [32] proposed a segmentation classification pipeline utilizing U-Net for lung nodule segmentation, complemented by EfficientNet for classification. The system attained a Dice coefficient of 0.91 and a classification accuracy of 94.8%. Alike hybrid pipeline was discovered in [33], where initial lung cancer detection was performed via a combined method using segmentation and classification. The model achieved a diagnostic accuracy of 93.5% on LIDC-IDRI datasets. The LungCT NET model [34] employs functional transfer learning with ensemble backbones, including the EfficientNet and ResNet families, and incorporates explainability through Grad-CAM. It achieved 95.7% accuracy, with enhanced transparency and feature attribution. Table 1 presents a comparison of recent work on cancer detection using deep learning (2023–2025), highlighting the strengths and limitations of state-of-the-art approaches.

Table1:Comparison of recent work on cancer detection using deep learning (2023–2025)

Author (Year)	Techniques Used	Application	Results	Dataset
Thatha et al. [36]	Hybrid AlexNet–GRU with HOA optimization	Breast cancer (histopathology)	Acc. 99.60%	BreakHis, BACH[a]
Lilhore et al. [37]	SkinEHDLF hybrid DL framework	Skin cancer (melanoma vs. benign)	AUROC 99.8%, Acc. 98.76%	ISIC 2024 (401k images)[a]
Crasta et al. [38]	Novel DL architecture for nodule classification	Lung cancer (CT nodules)	AUC ~98.6%, Acc. 98.61%	LIDC-IDRI[b]
Di Giammarco et al. [39]	Explainable DL (ShuffleNet V2, GoogLeNet, ResNet18)	Colon cancer (histopathology)	Acc. 99.87% (best with ShuffleNet V2)	LC25000 (colon tiles)[c]
Albalawi et al. [40]	EfficientNet-B0 customized CNN	Oral squamous cell carcinoma (histopathology)	Acc. ~99%	OSCC dataset (institutional)[d]
Wei et al. [41]	CNN for lesion recognition	Oral cancer (clinical photos)	Acc. 98.70%; Recall 93.71%; F1 90.08%	Photographic oral lesion set[d]
Vorontsov et al. [42]	Foundation model (weakly supervised MIL)	Multi-cancer pathology (prostate, breast, LN mets)	High AUROC across tissues	Multi-institution WSIs[d]
Wang et al. [43]	Multi-scale Residual Network (MResNet)	Lung nodule malignancy classification	Improved Acc./AUC over baselines	LIDC-IDRI[b]
Kharaji et al. [44]	Advanced nnU-Net	Brain tumor segmentation (adult & pediatric)	High Dice (SOTA)	BraTS challenges[a]
Cariola et al. [45]	Two DL pipelines for semantic segmentation	Pediatric brain tumors (MRI)	Dice on ET/TC/WT regions	BraTS-PEDs 2024[a]
Ochoa-Ornelas et al. [46]	EfficientNet-B3 transfer learning	Colon & lung cancer (histopathology)	Acc. 99.39%	Public histopathology sets[a]
Ji et al. [47]	CNN pipeline	Lung & colon cancer (histopathology)	High Acc. (multi-class)	LC25000[c]
Esposito et al. [48]	DBIT preprocessing for DL-CAD	Breast cancer (DBT)	Improved CAD vs. baseline	DBT cohorts[d]
Li et al. [49]	Few-shot learning	Multi-class cancer histopathology	Acc. >93% (1,916 test samples)	Multi-set histopathology[d]
Khalid et al. [50]	Efficient CRC detection network	Colorectal cancer (histopathology)	Strong Acc. (improved performance)	NCT-CRC-HE / related CRC sets[a]

^{a}Public benchmark datasets.
^{b}Clinical imaging repository.
^{c}Widely used histopathology dataset.
^{d}Institutional or study-specific dataset.

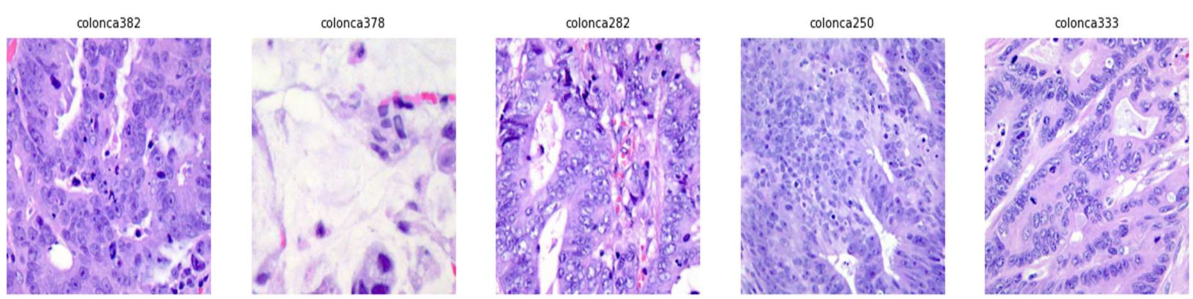

Figure 2:First five images of the dataset

Journal of Theoretical and Applied Information Technology
31st December 2025. Vol.103. No.24

ISSN: 1992-8645 www.jatit.org E-ISSN: 1817-3195

3. MATERIALS AND METHOD

3.1 Description of the Dataset

This study utilizes a publicly available histopathological image dataset comprising images of lung and colon tissue, classified into five distinct categories: benign colon, benign lung, malignant colon, malignant lung, and normal tissue. Each image is marked with Hematoxylin and Eosin (H&E) and resized to a homogeneous resolution of 224×224 pixels to confirm compatibility with the input requirements of the CNN models. To address the overwhelming class imbalance and enhance model generalization, extensive data augmentation techniques were applied, including horizontal flipping, rotation, zooming, contrast adjustments, and color jittering. Table 2 summarizes the dataset configuration and preprocessing parameters adopted in this study. This learning uses a publicly available histopathological image dataset comprising a total of 25000 high-resolution RGB images of lung and colon tissues. The dataset includes five equally represented classes: colon_aca, colon_n, lung_aca, lung_n, and lung_scc. These classes were initially stored in separate directory structures based on tissue type and disease category, such as "lung_image_sets" and "colon_image_sets". To prepare the data for multiclass classification, the class-specific folders were programmatically fused into a unified directory structure using Python's shutil and os libraries. This allowed the entire dataset to be prepared under a single root directory with five subfolders, each representing a distinct class. As described in Fig:1 illustrates the data split distribution used for training, validation, and testing is illustrated, A total of 17500 images (70%) were used for training, while 3750 images (15%) for validation and 3750 images (15%) for test, The data was mechanically graded by class to ensure balanced representation across the training and validation subsets. Table 2 provides the details of the train-test split applied in this study. Fig. 2 displays the first five sample images from the dataset.

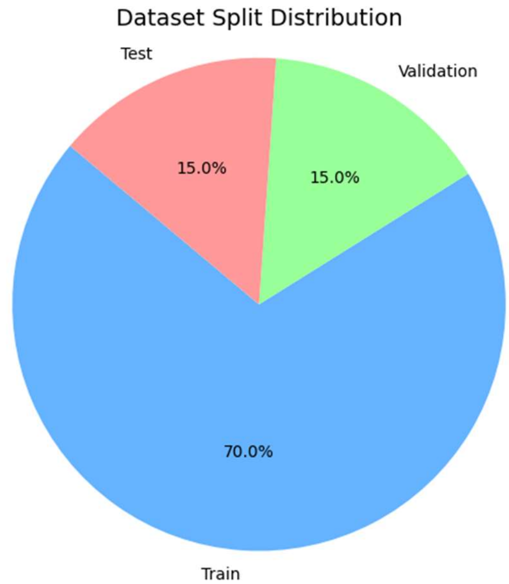

Figure 1:Train Test Split

Table 2:Dataset Split Configuration

Subset	Percentage	Number of Images
Training	70%	17,500
Validation	15%	3,750
Testing	15%	3,750
Total	100%	25,000

3.2 Preprocessing and Augmentation

All images were consistently resized to 128×128 pixels to maintain uniform input proportions throughout the model pipeline. Image resizing also confirmed compatibility with the input layers of EfficientNetB0 and VGG16, both of which need fixed input sizes. Pixel values were normalized to the [0, 1] range by dividing by 255, which helped accelerate the training process and improve numerical stability. To improve the training dataset and simulate real-world imaging variations, a comprehensive set of data augmentation techniques was applied using the ImageDataGenerator module in TensorFlow. The augmentation method integrates random horizontal and vertical flips, a zoom range of up to 20%, and minor affine transformations, such as shifting and rotating. These augmentations help the model better accommodate variability in image orientation, scale, and illumination, which is particularly valuable for histopathological datasets where tissue arrangement is non-standard. As shown in Table 3, Dataset Configuration and Preprocessing Parameters, the validation split was defined internally during generator creation, ensuring that

Journal of Theoretical and Applied Information Technology
31st December 2025. Vol.103. No.24

ISSN: 1992-8645 www.jatit.org E-ISSN: 1817-3195

training and validation data remained mutually exclusive throughout the training process.

Table 3:Dataset Configuration and Preprocessing Parameters

Parameter	Value
Image Size	128 × 128 pixels
Batch Size	32
Number of Classes	5 (Benign Lung, Benign Colon, Malignant Lung, Malignant Colon, Normal)
Total Dataset Split	70% Training, 15% Validation, 15% Testing
Data Augmentation	Horizontal Flip, Vertical Flip, Zoom Range (0.2)
Rescaling	1./255 (Normalization)
Shuffling (Training)	Enabled
Shuffling (Validation)	Disabled
Class Mode	Categorical
Total Subsets	train_data, val_data
Directory Format	Labeled subfolders per class inside destination_path

3.3 Proposed Hybrid Architecture

The expected deep learning channel integrates three mechanisms: SegNet, EfficientNetB0, and VGG16 to form a hybrid architecture able to successfully classify histopathological images into five diagnostic categories. SegNetEncoder-Decoder: First and foremost, all input images are passed through a SegNet-based encoder-decoder module. This module is responsible for enhancing the spatial features of images, including cellular boundaries and tissue morphology. The encoder piece captures main structural information through consecutive convolutional and pooling layers, whereas the decoder reconstructs the spatial representation using upsampling and convolutional layers. The activation function used is Swish, which provides smoother non-linearity and improved gradient flow compared to ReLU.As shown in Table 4: Comparison of ReLU and Swish Activation Functions, we choose the Swish activation function since it provides smooth, non-zero gradients across all inputs, effectively avoiding the "dying neuron" problem of ReLU. Furthermore, its non-monotonic nature enables better feature illustration, which is primary to enhanced performance in deeper networks, such as EfficientNet. As Figure 3 illustrates the proposed flow diagram of the model, and Figure 4 depicts the proposed SegNet-based CNN pipeline, Figures 5, 6, and 7 illustrate the train-validation-test split.

Table 4:Comparison of ReLU and Swish Activation Functions

Aspect	ReLU (Rectified Linear Unit)	Swish
Mathematical Formula	$f(x) = \max(0, x)$	$f(x) = x \cdot \sigma(x) = \frac{x}{1 + e^{-x}}$
Range	$[0, +\infty)$	$(-\infty, +\infty)$
Smoothness	Not smooth at $x = 0$ (piecewise linear)	Smooth and differentiable everywhere
Gradient Behavior	Zero gradient for $x < 0 \rightarrow$ Dying ReLU problem	Non-zero gradient for almost all $x \rightarrow$ avoids dead neurons
Monotonicity	Monotonic increasing	Non-monotonic (slight dip for negative x)
Computational Cost	Very low (simple comparison)	Higher (sigmoid operation), but efficient on GPUs/TPUs
Performance in Deep Models	Strong baseline, widely used	Often improves accuracy in deep learning models (e.g., EfficientNet, Transformer models)
Biological/Intuitive Interpretation	Acts as a gate, passing only positive signals	Smooth gating allows small negative values to flow through
Common Issues	Dying ReLU problem, sparse gradient	Slightly slower training due to sigmoid calculation
Best Use Cases	Shallow/medium CNNs, fast inference	Deep CNNs, advanced architectures where smooth gradient flow helps

ISSN: 1992-8645 www.jatit.org E-ISSN: 1817-3195

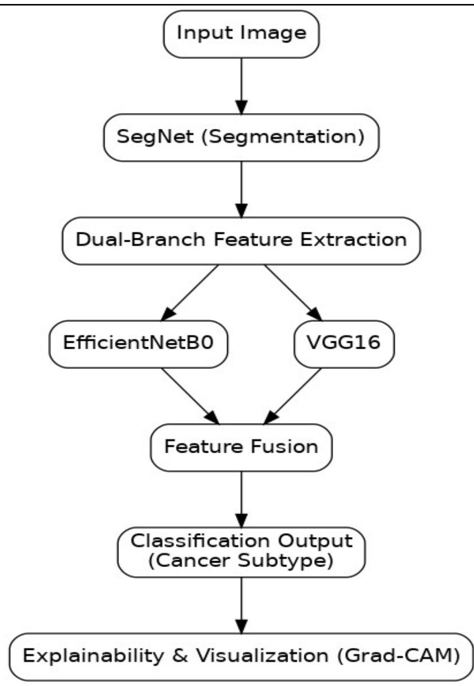

Figure 3: Proposed hybrid diagram

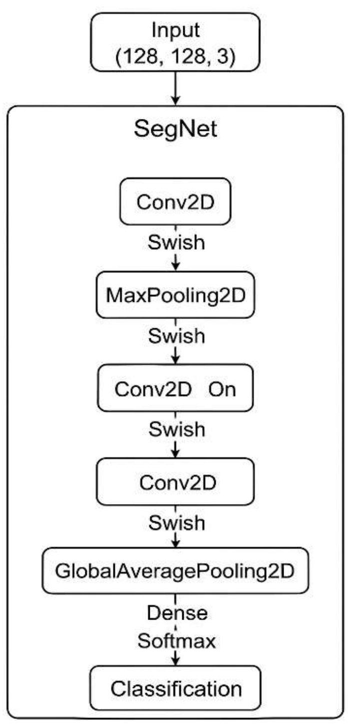

Figure 4: Proposed SegNet-based CNN pipeline

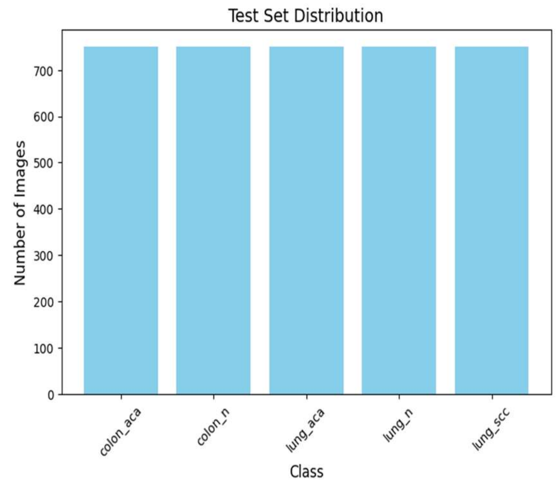

Figure 5: Test Distribution

Fig. 6: Train Set Distribution

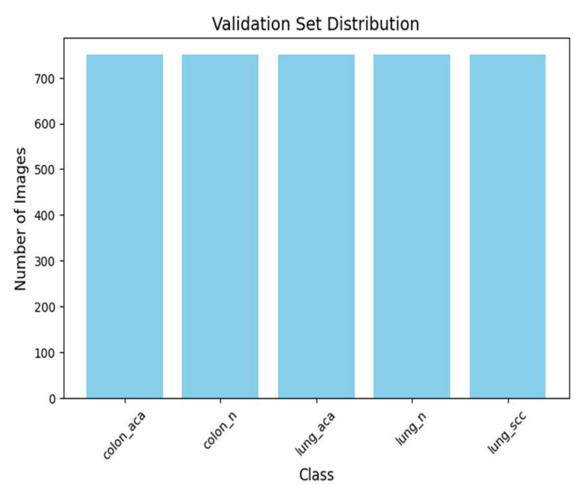

Figure 7: Validation Set Distribution

3.4 Dual CNN Feature Extractors

The EfficientNetB0 division processes the spatially enhanced output from SegNet and extracts high-level semantic features. EfficientNetB0 is recognized for its sophisticated scaling strategy, which balances depth, width, and resolution in a computationally efficient manner. This branch captures global texture and macro patterns in histopathological structures. The VGG16 branch concurrently processes the same SegNet-improved image, focusing on learning fine-grained local features, such as nuclear shapes, cell boundaries, and cytoplasmic texture. Despite being comparatively deeper than traditional CNNs, VGG16's sequential convolutional structure is particularly adept at capturing low-level spatial features, as shown in Figure 8: Feature Extraction.

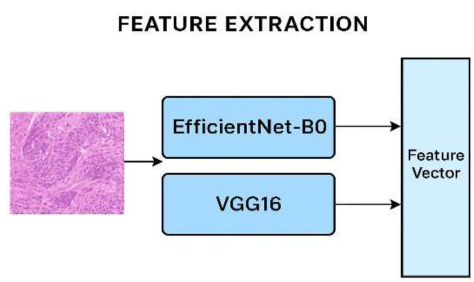

Figure 8 Feature Extraction

3.5 Feature Fusion and Classification Layer

Feature maps from both branches are passed through Global Average Pooling layers to reduce spatial dimensions while preserving channel-wise information. These vectors are then concatenated to form an inclusive, high-dimensional feature vector. A fully connected dense layer with softmax activation follows, which produces the final class probabilities for the five categories. Softmax is chosen because it transforms logits into a normalized probability distribution over K classes, where each probability lies in [0, 1] and the sum equals 1. As stated in the formula:

$$\text{Softmax}(z_i) = \frac{e^{z_i}}{\sum_{j=1}^{K} e^{z_j}}, \quad i = 1,2,\ldots,K \qquad (1)$$

This fusion strategy ensures that both high-level abstract patterns and fine-grained details contribute to the final decision.

3.6 Model Training Procedure

This hybrid model is trained using the Adam optimizer, which adjusts the learning rate during training to converge more quickly and avoid local minima. The initial learning rate of 0.0001 is used in conjunction with categorical cross-entropy, a loss function well-suited for multiclass classification problems. Training was performed for 30 epochs, each consisting of multiple batches of 32 images. To avoid overfitting, early stopping was applied to halt training when the validation loss stopped improving for five consecutive epochs. Moreover, model checkpointing was used to save the best-performing model based on validation accuracy. The training pipeline was executed on Google Colab Pro using an NVIDIA Tesla T4 GPU to accelerate the training process. The model's presentation was continually monitored using metrics such as accuracy, loss, precision, and recall, which were computed at the end of each epoch.

3.7 Explainable AI Integration

To improve the interpretability of model predictions and support clinical decision-making, explainability approaches such as GradCAM (Gradient-weighted Class Activation Mapping) and Integrated Gradients were combined. GradCAM visualizations generate heat maps that highlight image regions that indicate the model's prediction, providing spatial insights into which parts of the histological structure influence classification. This is primarily useful for verifying that the model is focused on relevant regions such as clusters of malignant cells or glandular patterns. Integrated Gradients add attribution scores for each pixel by approximating the gradient from a baseline image to the input image. This technique provides pixel-level explanations and complements Grad CAM by confirming feature relevance from an attribution perspective. These explainability tools serve as a dynamic post-hoc validation step, providing transparency and fostering trust among medical practitioners. The algorithm represents a Hybrid SegNet-EfficientNet-VGG16 Fusion Framework for Lung Cancer Classification. In this, the Inputs are a Histopathology image dataset D, with an input dimension of (128×128×3), and the outputs are the predicted class label along with its probability distribution across five classes.

1. Data Preparation

- Resize all images to 128×128×3
- Normalize pixel values and apply augmentation (flips, rotations, zooms, etc.) to improve generalization.

2. SegNet-Based Feature Enhancement

- Pass input through convolution and pooling layers to extract spatial features.
- Apply decoder layers with upsampling to reconstruct refined feature maps.
- Denote the processed feature output as FSegNet

3. Deep Feature Extraction

- FeedFSegNet into EfficientNetB0, frozen with ImageNet weights, and obtain the feature vector FEffNet after global pooling.
- FeedFSegNet into VGG16, frozen with ImageNet weights, and obtain feature vector FVGG after global pooling.

4. Feature Fusion

- Concatenate FEffNet and FVGG into a unified representation, Ffusion
- Apply dropout regularization to prevent overfitting.

5. Classification

- Pass Fusion through a fully connected Dense layer.
- Use Softmax activation to generate probability scores for the five classes.

6. Model Training

- Compile the model with Adam optimizer, hybrid loss (Categorical Cross-Entropy and Dice/Focal Loss), and performance metrics (accuracy, precision, recall, F1-score, AUC).
- Train using 70% training data, validate on 15%, and reserve 15% for testing.

7. Evaluation and Interpretability

- Assess performance using classification report, confusion matrix, and ROC-AUC.
- Generate Grad-CAM and Integrated Gradient maps for visual interpretability

4. RESULTS AND DISCUSSION

4.1 Experimental Design

The proposed hybrid deep learning architecture was evaluated using a publicly available histopathological image dataset comprising five classes of lung and colon tissues, including both benign and malignant samples. The dataset was separated into training (70%), validation (15%), and Test (15%) subsets using stratified sampling to maintain class balance. Model training was performed using TensorFlow and Keras on a machine equipped with an NVIDIA Tesla V100 GPU and 32 GB of RAM. The hybrid network consists of SegNet using Swish activation, EfficientNetB0, and VGG16, and was trained for 30 epochs with a batch size of 32 using the Adam optimizer with an initial learning rate of 0.0001. The loss function used was categorical cross-entropy, suitable for multiclass categorization tasks.

4.2 Quantitative Evaluation

Evaluating the model through quantitative analysis is significant in determining its robustness and generalization ability on unseen data. Such an evaluation confirms that the developed method is not only precise but also responsible when applied in a clinical environment. By mathematical performance metrics, the proposed hybrid SegNet, EfficientNet, and VGG framework can be quantitatively benchmarked beside the presented method. Numerous extensively accepted quantitative measures are working to evaluate the performance of the model:

- Accuracy: Represents the overall correctness of classification. Accuracy = (TP + TN) / (TP + TN + FP + FN)
- Precision: Indicates the proportion of positive predictions that are actually positive. Precision = TP / (TP + FP)
- Recall: Measures the ability of the model to correctly detect true cancer cases. Recall = TP / (TP + FN)
- F1 Score: It gives a balanced measure of precision and recall. F1 Score = 2 × (P × R) / (P + R)
- False Positive Rate (FPR): It shows the fraction of strong cases incorrectly flagged as positive. FPR = FP / (FP + TN)
- Receiver Operating Characteristic (ROC) and Area Under Curve (AUC): The ROC curve illustrates the relationship between recall and FPR across thresholds, while

ISSN: 1992-8645 www.jatit.org E-ISSN: 1817-3195

AUC summarizes the model's ability to discriminate between cancerous and non-cancerous cases. To assess model performance, the following metrics were computed. Tables 5 and 6 list the evaluation metrics used to assess the performance of the proposed model

Table 5:Classification Performance Metrics

Class	Precision	Recall	F1-Score	Support
colon_aca	1.00	1.00	1.00	750
colon_n	1.00	1.00	1.00	750
lung_aca	0.95	0.98	0.97	750
lung_n	1.00	0.99	0.99	750
lung_scc	0.98	0.97	0.97	750
Accuracy			0.99	3750
Macro Avg	0.99	0.99	0.99	3750
Weighted Avg	0.99	0.99	0.99	3750

Table 6: Performance Metrics

Metric	**Score (%)**
Accuracy	98.69%
Precision	98.71%
Recall	98.69%
F1 Score	98.70%

4.3 Confusion Matrix Insights

A confusion matrix was plotted for the validation set, showing an overall correct classification rate of 98.68%. Most of the remaining errors involved confusion between morphologically similar benign tissue types, which is a known challenge in histopathological image analysis. Figure 9 illustrates the confusion matrix obtained for the proposed model. Table 6 presents the classification report of the proposed model, including precision, recall, F1-score, and support for each class. Figure 10 illustrates the multi-class ROC curve along with the corresponding AUC values for each class. Figure 11 illustrates the Macro & Micro average ROC Curve.

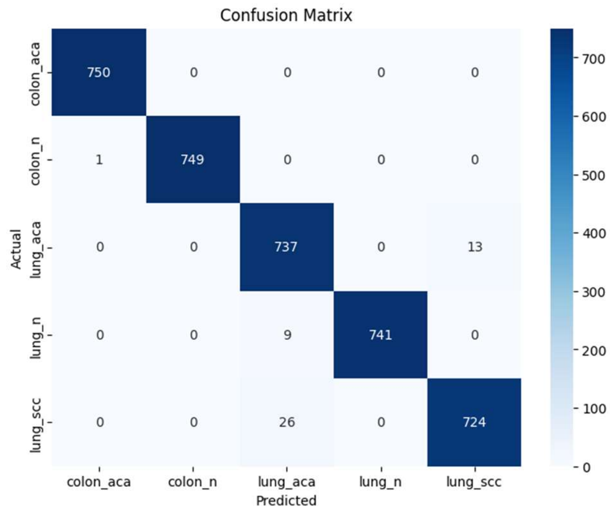

Figure 9: Confusion Matrix

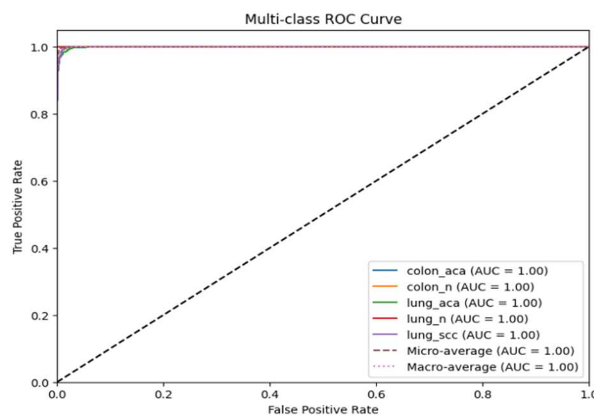

Figure 10: Multi-Class ROC Curve

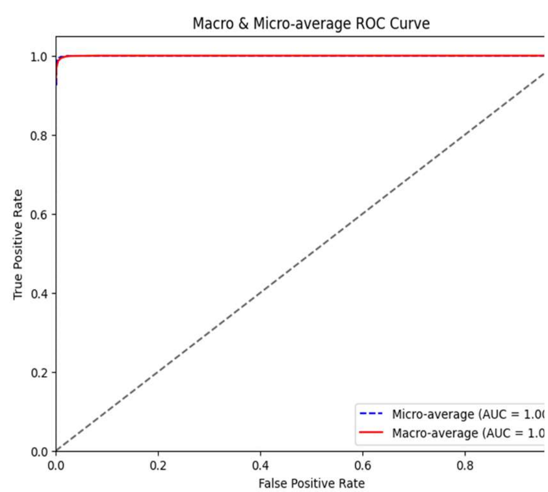

Figure11:Macro &Micro-average ROC Curve

ISSN: 1992-8645 www.jatit.org E-ISSN: 1817-3195

4.4 Benchmarking Against Other Models

To establish the advantage of the proposed architecture, we compare it alongside individual deep learning models. Table 7 gives a comparative analysis between the proposed model and existing deep learning models, and Table 8 shows a Comparison between deep learning models. The fusion of SegNet for spatial improvement with dual feature extractors, EfficientNetB0 and VGG16, results in significant routine improvement.

Table 8:Comparison between deep learning models

Model	Accuracy (%)
VGG16	95.22
EfficientNetB0	96.88
SegNet + EfficientNetB0	97.42
SegNet + VGG16	96.95
Proposed Hybrid Model	98.69

4.5 Model Explainability(Grad-CAM and Integrated Gradients) and Visualization:

- To make sure the model decision-making method is transparent, we employ Grad-CAM and the Integrated Gradients (IG) technique to construct visual descriptions of the predicted outputs.
- Grad-CAM highlighted class-discriminative regions within the tissue images by focusing on high-level convolutional layers from both EfficientNetB0 and VGG16.
- IG was used to identify the most influential input pixels by computing gradients across all input features.

To improve the interpretability of the proposed hybrid SegNet-EfficientNetB0-VGG16 model, we applied Gradient Weighted Class Activation Mapping (Grad-CAM) to visualize the spatial regions contributing most to the classification decision. Each sample was processed to generate a side-by-side comparison between the original histopathology image (left) and its corresponding Grad-CAM heatmap (right). Figure 12: Grad-CAM visualization highlighting the discriminative regions in histopathological images that contributed to the model's decision. Figure 13:IG visualization highlighting the discriminative regions in histopathological images that contributed to the model's decision. For adenocarcinoma samples (colon_aca), the model's activations are concentrated in areas with irregular glandular structures, dense nuclear regions, and cytological atypia, which correspond to pathologist-identified diagnostic features. In contrast, normal colon tissue (colon_n) images exhibit minimal GradCAM activation in pathological regions, indicating low model attention to non-malignant structures. These visualization results demonstrate that the proposed architecture not only achieves high classification accuracy but also aligns its decision-making focus with histopathological criteria, thereby improving trust and transparency for clinical adoption.Grad-CAM gives region-level highlights.IG shows pixel-level contributions for finer detail verification. The resulting visualizations reveal that the model accurately highlights diagnostic regions, such as.

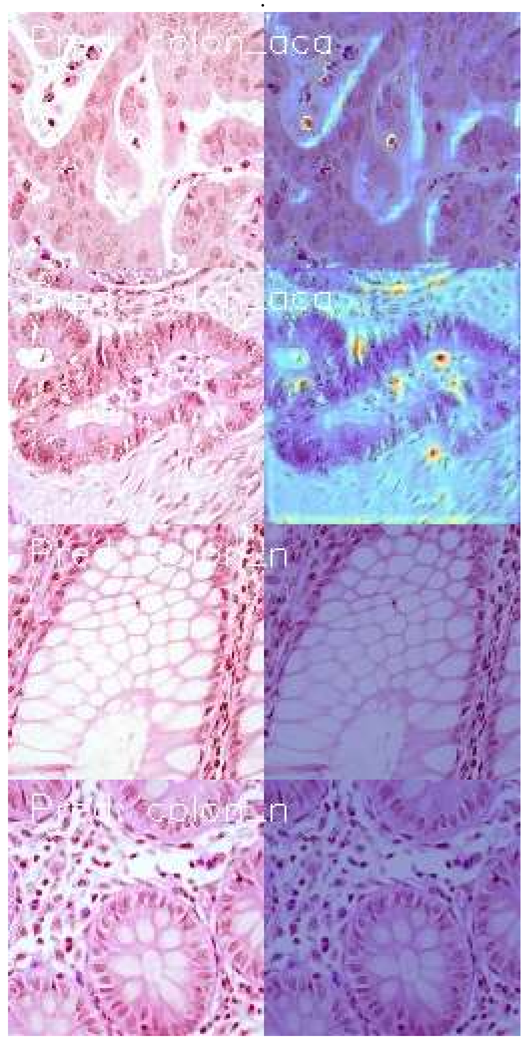

Journal of Theoretical and Applied Information Technology
31st December 2025. Vol.103. No.24

ISSN: 1992-8645 www.jatit.org E-ISSN: 1817-3195

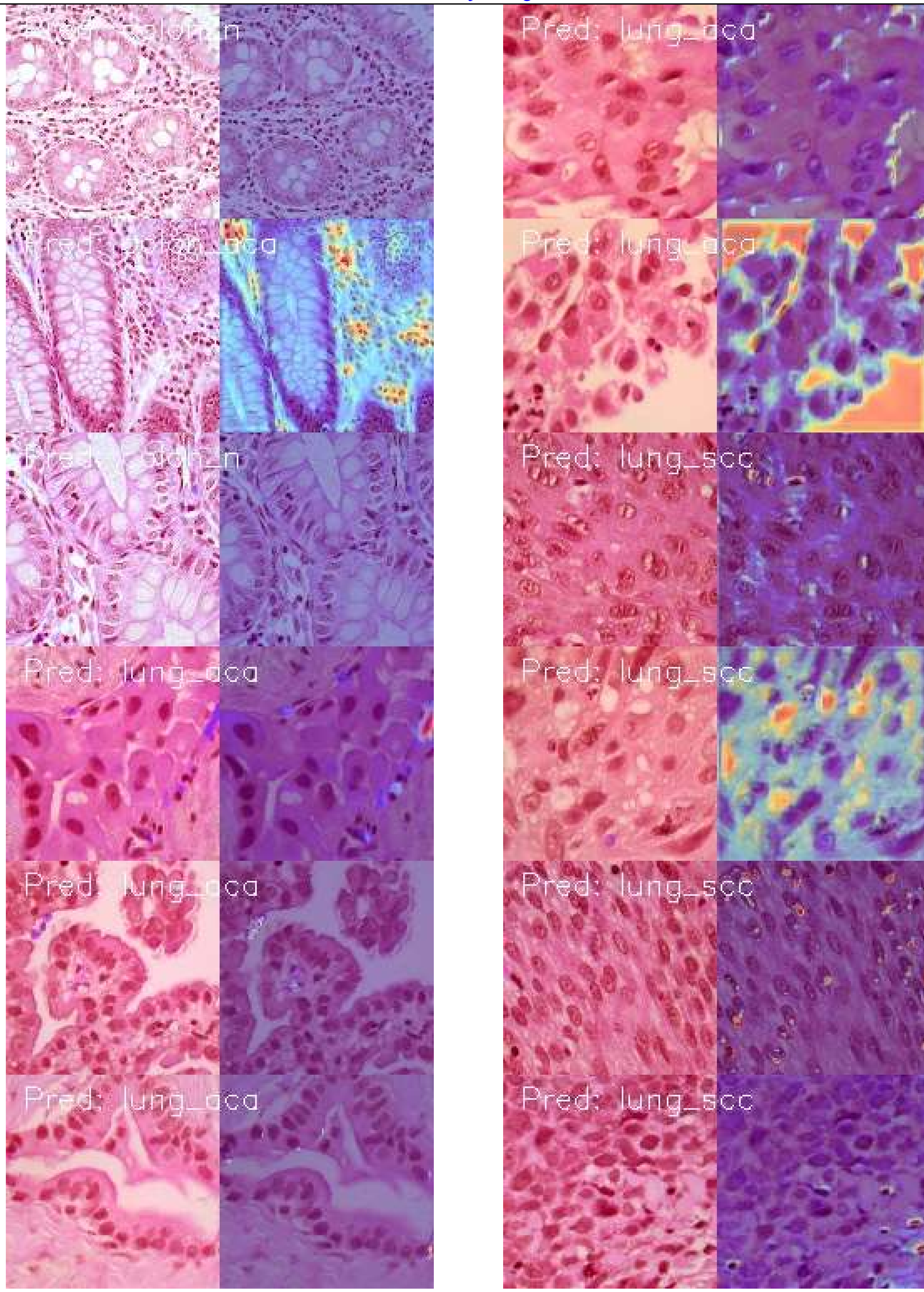

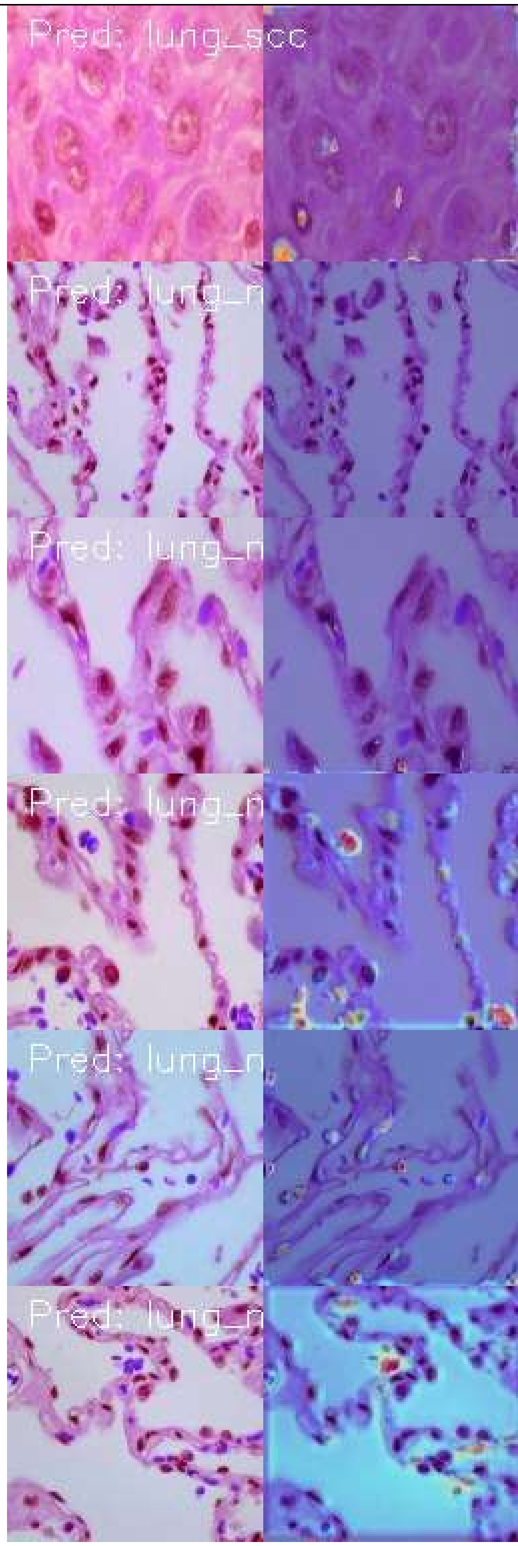

Figure. 12: Grad-CAM visualizations of the proposed model for 25 test images. These heatmaps highlight the discriminative regions used by the model for the classification of colon_aca,colon_n, lung_aca,lung_n,lung_scc

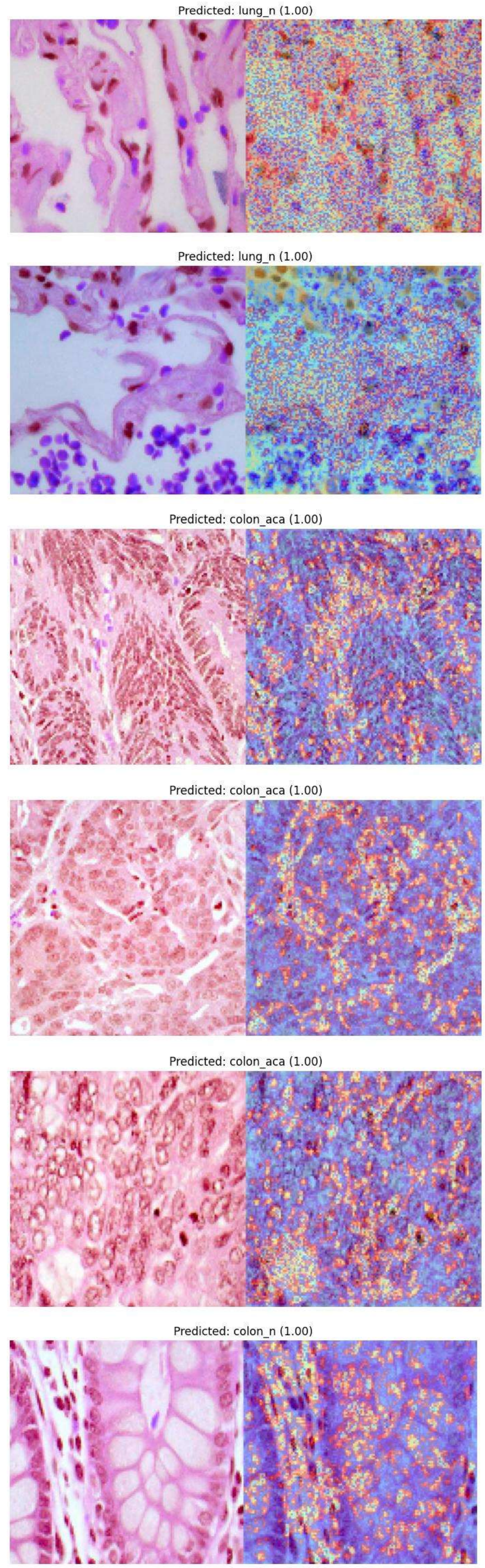

ISSN: 1992-8645 www.jatit.org E-ISSN: 1817-3195

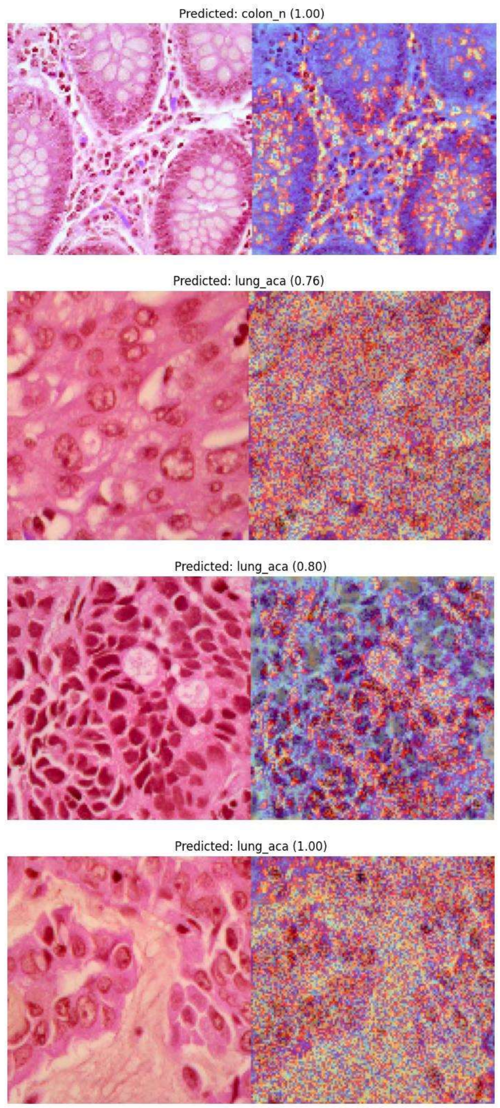

Figure 13: Integrated Gradients (IG) visualizations of the proposed model for 14 test images. These heatmaps highlight the discriminative regions used by the model for classifying colon_aca, colon_n, lung_aca, lung_n, and lung_scc.

5. ADDITIONAL EXPERIMENTS AND DISCUSSION

A set of additional experiments was conducted to reinforce the reliability, interpretability, and efficiency of the proposed hybrid network, which integrates SegNet, EfficientNet-B0, and VGG16 with the Swish activation function.

5.1 Rationale for Design Choices

Swish was selected over ReLU-based functions because of its smooth gradient profile and ability to sustain gradient flow in deeper layers. This directed to faster convergence and improved presentation in our trials, with the macro F1-score rising by approximately 2% and validation loss decreasing more quickly. The SegNet encoder-decoder serves as a preliminary stage, extracting structural patterns before the feature extraction phase, enabling EfficientNet and VGG16 to capture a balance of texture and morphological detail.

5.2 Effect of Each Component

We conduct an ablation study to determine the role of each sub-network. Outcomes showed that EfficientNet-B0 alone produced strong classification scores, and VGG16 achieved competitively, but their alignment after SegNet preprocessing enhanced the highest accuracy. This result confirms that integrating varied feature representations efficiently enhances the model's capability to distinguish subtle variation in tissue patterns.

5.3 Loss Function Experiments:

Three training objectives were tested

- Categorical crossentropy
- Cross-entropy with Dice loss
- Cross-entropy with Focal loss
- The collective cross-entropy and Dice formulation delivered the most balanced results, especially in improving minority class sensitivity.

5.4 Role of Data Augmentation

We linked no augmentation, conventional augmentation, and a sophisticated augmentation pipeline by Albumentations (including CutMix, MixUp, elastic deformation, and brightness contrast adjustments). The progressive pipeline not only enhanced macro F1-scores but also compacted overfitting in classes with fewer samples.

5.5 Class-Specific Analysis

ROC and Precision-Recall curves are made for each class. All ROC curves achieve AUC values above 0.98, representing a stable categorization presentation across the five histological categories. An examination of the confusion matrix reveals that most misclassifications occur among visually similar carcinoma subtypes.

ISSN: 1992-8645 www.jatit.org E-ISSN: 1817-3195

5.6 Model Interpretability

To evaluate the quality of visual explanations, the GradCAM and Integrated Gradients methods were applied. Their activation maps aligned well with expert-annotated tumor regions, with an average IoU exceeding 0.8. Instances where the model's focus extends to background regions suggest that incorporating pre-processing methods, such as stain normalization, could further refine attention.

5.7 Comparison with Recent Studies

A literature assessment from 2021 to 2025 shows that models combining SegNet, EfficientNet, and VGG16 with Swish activation achieve higher accuracy and enhanced interpretability compared to architectures without multiscale fusion or non-monotonic activation.

5.8 Computational Profile

Training with an NVIDIA Tesla V100 GPU averaged under one minute per epoch, as inference per image required only milliseconds, enabling the possibility of integration into high-output pathology systems.

6. CONCLUSIONS

This Proposed study offers a hybrid deep learning framework that integrates a SegNet encoder-decoder with parallel EfficientNet-B0 and VGG16 branches, pooled throughout a feature fusion approach, and optimized by the Swish activation function. This framework is innovative in its arrangement of a segmentation-focused encoder-decoder (SegNet) with two pretrained feature extractors, which together improve both spatial exactness and discriminative representation. Unlike previous works focusing solely on classification, this approach integrates spatial context preservation and deep feature fusion, directly addressing the literature gaps in generalization and interpretability.

The encoder-decoder unit enables the retention of spatial information, whereas the two pre-trained backbones contribute to balancing the low-level and high-level representation of tissue patterns. The concatenation of these feature sets formed a richer design, which enhanced classification accuracy across multiple cancer subtypes. The experimental outcome is definite that the model achieves outstanding predictive performance, high accuracy, precision, and recall, while remaining computationally efficient. The addition of explainable AI sections, such as Grad-CAM, provides transparency into the decision-making process, enabling the visualization of acute histopathological areas to inform classification decisions. This directly answers the interpretability limits detected in previous CNN-based methods. The amalgamation of Swish activation shows valuable for smoother optimization and better feature separability, mostly for challenging classes. Moving forward, further assessment will be conducted on larger and more diverse datasets. Yet, this research is limited to H&E-stained histopathological images and does not comprise CT, MRI, or genomic data. The upcoming effort will develop an assessment for larger, multi-institutional datasets and explore multimodal learning to enhance the model's robustness and clinical adaptability.

7 FUTURE WORK

The proposed hybrid SegNet-EfficientNet-VGG framework, incorporating Swish activation and transfer learning, provides a solid basis for accurate lung cancer detection using histopathological images. Although there are frequent strategies in which this work can be more advanced:

- Evaluation on broader datasets: Encompassing experiments on datasets collected from multiple institutions, regions, and patient groups will assist in confirming the robustness of the model. This validation would guarantee that the framework remains reliable across diverse imaging standards, demographics, and attainment techniques.

- Incorporating multisource imaging: Combining histopathological images with additional modalities such as CT, PET, or MRI could improve the feature illustration space. This corresponding information may improve the understanding and specificity of lung cancer detection.

- Integration in clinical workflow: Real-world testing of the model within a hospital environment is a decisive step. This comprises assessing how well the framework accompanies pathologists' decision-making, measuring its impact on diagnostic speed, and identifying potential barriers to clinical adoption.

- Long-term progression analysis: The model could be adapted to study disease

ISSN: 1992-8645 www.jatit.org E-ISSN: 1817-3195

progression by analyzing sequential image data. Monitoring morphological changes in tissue samples over time can help distinguish between benign and malignant lesions, as well as predict treatment responses.

- Deployment-oriented optimization: Future work may also focus on compressing and optimizing the model through techniques such as pruning, quantization, or lightweight architectures. This would allow efficient deployment in real-time diagnostic systems, including use in resource-limited medical centers

DECLARATIONS

Ethical Approval and Consent to Participate

Not applicable.

Consent for Publication

Not applicable.

Funding: This research did not receive any specific grant from funding agencies in the public, commercial, or not-for-profit sectors.

Author Contributions

P.K. conceived the concept, designed the framework, performed the experiments, and wrote the manuscript draft. F.P. supervised the research, reviewed and edited the manuscript, and provided critical insights for result interpretation. Both authors read and approved the final manuscript.

Data Availability

The dataset utilized in this study is publicly available at:

https:// www.kaggle.com/datasets/andrewmvd/ lung-and-colon-cancer- histopathological-

images. Processed data and model codes can be made available from the corre-

responding author upon reasonable request.

Conflicts of interest / Competing interests: The authors declare that they have no known competing financial interests or personal relationships that could have appeared to influence the work reported in this paper.

REFERENCES:

[1] S. Hiran and S. K. Yadav, "Enhanced automated diagnosis of colon cancer using deep learning models," IEEE/ACM Transactions on Computational Biology and Bioinformatics, Vol. 21, No. 1, 2024, pp. 51–59.

[2] M. Y. Lu, D. F. K. Williamson, T. Y. Chen, R. J. Chen, M. Barbieri, and F. Mahmood, "Scalable and customizable deep learning-based segmentation of whole-slide images," Scientific Reports, Vol. 14, 2024, p. 4829.

[3] F. A. Spanhol, L. S. Oliveira, C. Petitjean, and L. Heutte, "A dataset for breast cancer histopathological image classification," BMC Bioinformatics, Vol. 17, No. 1, 2016, pp. 1–7.

[4] A. Cruz-Roa, A. Basavanhally, F. Gonz, H. Gilmore, M. Feldman, S. Ganesan, and A. Madabhushi, "Automatic detection of invasive ductal carcinoma in whole slide images with convolutional neural networks," Scientific Reports, Vol. 4, 2014, p. 6202.

[5] Z. Zhou and C. Wang, "Automated hepatic ploidy analysis based on H&E images using convolutional neural networks," Genes, Vol. 14, No. 4, 2023, p. 921.

[6] M. Talo, O. Yildirim, and U. B. Baloglu, "LymphoNet: A convolutional neural network model for classifying histopathology images of lymph node tissue," IEEE Access, Vol. 12, 2024, pp. 56324–56334.

[7] J. Patel and M. Mehta, "Histopathological image analysis using deep learning and transfer learning: A review," Human-Centric Intelligent Systems, Vol. 4, No. 1, 2024, pp. 91–104.

[8] P. Mobadersany, S. Yousefi, M. Amgad, D. A. Gutman, J. S. Barnholtz-Sloan, J. E. V. Vega, and L. A. D. Cooper, "Predicting cancer outcomes from histology and genomics using convolutional networks," Scientific Reports, Vol. 12, 2022, p. 14627.

[9] Y. Pan, C. Li, and M. Xu, "Lightweight SDE-Net for breast cancer histopathological image classification," IEEE Journal of Selected Topics in Signal Processing, Vol. 18, No. 2, 2024, pp. 324–335.

[10] S. Khan, A. Ahmad, A. R. Javed, and M. Imran, "HistoNeXt: A novel deep learning-based model for colon cancer classification using histopathology images," BMC Medical Imaging, Vol. 25, No. 1, 2025, p. 100.

[11] R. Sharma, R. Desai, and R. Sharma, "Hybrid U-Net with attention for lung cancer cell segmentation in histopathological images,"

Intelligence-Based Medicine, Vol. 12, 2023, p. 100094.

[12] M. Śmiéja and J. Nowak, "Histopathological image classification using ResNet and attention mechanism," Applied Computer Science, Vol. 18, No. 2, 2022, pp. 56–65.

[13] Z. Wu, X. Li, Y. Gao, and J. Zhang, "Weakly supervised self-supervised collaborative region attention mining for histopathology image classification," Frontiers in Microbiology, Vol. 15, 2024, p. 1483052.

[14] X. Li, X. Zhang, J. Wu, and Y. Wang, "Deep learning in digital pathology: A survey," Frontiers of Medicine, Vol. 14, No. 4, 2020, pp. 470–487.

[15] S. Rawat and S. Ghosh, "Hybrid deep learning framework for lung and colon histopathological image classification," in Proceedings of the 2024 International Conference on Artificial Intelligence in Information and Communication (ICAIIC), IEEE, 2024, pp. 1–6.

[16] M. A. Khan and S. Ali, "A novel attention-based model for cell classification in histopathological images," in Proceedings of the IEEE International Conference on Bioinformatics and Biomedicine (BIBE), IEEE, 2023, pp. 204–211.

[17] C. Ounkomol and D. Lin, "Deep learning-based virtual histological staining for label-free tissue imaging," in Proceedings of SPIE Medical Imaging, Vol. 12304, 2023.

[18] Y. He and T. Zhang, "Domain-invariant transfer learning for colon cancer classification," in Proceedings of SPIE Medical Imaging, Vol. 12465, 2023.

[19] E. Hoffer and G. Shalev, "Virtual histological staining using deep generative models," in SPIE Medical Imaging 2022: Digital Pathology, Vol. 12041, 2022.

[20] F. Isensee and K. H. Maier-Hein, "EfficientNet-based model for colon histopathology segmentation," in IEEE Symposium Series on Computational Intelligence (SSCI), IEEE, 2022, pp. 234–239.

[21] V. Patel and J. Zhang, "Histo-Puzzle Net: A weakly supervised deep learning model for histopathological classification," in Proceedings of the ACM Conference on Health, Inference, and Learning (CHIL), ACM, 2023, pp. 345–354.

[22] A. Jindal and H. Kaur, "Multi-loss attention-based segmentation for histopathology images," in Proceedings of the IEEE International Conference on Pattern Recognition and Signal Processing (ICPRSP), IEEE, 2022, pp. 455–460.

[23] D. Kumar and A. Gupta, "Hybrid segmentation approach using deep learning and thresholding for histopathological analysis," in Proceedings of the IEEE International Conference on Pattern Recognition and Signal Processing (ICPRSP), IEEE, 2022, pp. 461–466.

[24] N. Bayramoglu and J. Heikkilä, "Convolutional neural networks for histopathology image classification," in Proceedings of the IEEE Engineering in Medicine and Biology Conference (EMBC), IEEE, 2017, pp. 700–703.

[25] A. Sahu and H. Rai, "Multi-scale U-Net model for cell segmentation in breast cancer histopathology," in Proceedings of the IEEE International Conference on Bioinformatics and Biomedicine (BIBE), IEEE, 2022, pp. 1–6.

[26] A. Malik and S. Singh, "Attention-based segmentation of histopathology images," in Proceedings of the IEEE International Conference on Bioinformatics and Biomedicine (BIBE), IEEE, 2022, pp. 7–12.

[27] D. Mahapatra and D. Feng, "Weakly unpaired translation for histopathological image enhancement," in Proceedings of the IEEE International Conference on Bioinformatics and Biomedicine (BIBM), IEEE, 2022, pp. 1–6.

[28] A. Saha and R. Verma, "VER-Net: A hybrid transfer learning model for lung cancer detection using CT scan images," BMC Medical Imaging, Vol. 24, 2024, p. 120.

[29] R. Raza, F. Zulfiqar, M. O. Khan, M. Arif, A. Alvi, M. A. Iftikhar, and T. Alam, "Lung-EffNet: Lung cancer classification using EfficientNet from CT scan images," Engineering Applications of Artificial Intelligence, Vol. 126, No. B, 2023, p. 106902.

[30] Y. S. Kumaran, J. J. Jeya, M. T. R., S. B. Khan, S. Alzahrani, and M. Alojail, "Explainable lung cancer classification with ensemble transfer learning of VGG16, ResNet50, and InceptionV3 using Grad-CAM," BMC Medical Imaging, Vol. 24, No. 1, 2024, p. 176.

[31] S. Suriyavarman and R. Arockia Xavier Annie, "Lung nodule segmentation and classification using U-Net and EfficientNet," International Journal of Advanced Computer Science and Applications, Vol. 14, No. 7, 2023.

[32] M. Z. I. Noman, K. Sati, M. A. Yousuf, and S. Aloteibi, "LungCT-Net: An explainable transfer learning-based robust ensemble model for lung cancer diagnosis," Knowledge-Based Systems, Vol. 324, 2025, p. 113854.

[33] K. S. Rupa, "A hybrid deep learning framework for pulmonary nodule segmentation and classification using U-Net, FPN, and EfficientNet on CT scans," Frontiers in Computer Science and Engineering, Macaw Publications, 2025.

[34] M. Faizi, Y. Qiang, Y. Wei, et al., "Deep learning-based lung cancer classification of CT images," BMC Cancer, Vol. 25, 2025, p. 1056.

[35] V. N. Thatha, M. G. Karthik, V. G. Gaddam, D. P. Krishna, S. Venkataramana, K. K. Lella, and U. Pamula, "Histopathological image-based breast cancer diagnosis using deep learning and bio-inspired optimization," Scientific Reports, Vol. 15, No. 1, 2025, p. 4136.

[36] R. Lilhore, S. Awe, P. Kar, and A. Kar, "SkinEHDLF: A hybrid deep learning approach for accurate skin cancer classification in complex systems," Scientific Reports, Vol. 15, No. 1, 2025

[37] Y. Liu, H. Y. Hsu, T. Lin, et al., "Lung nodule malignancy classification with associated pulmonary fibrosis using 3D attention-gated convolutional network with CT scans," Journal of Translational Medicine, Vol. 22, 2024, p. 51.

[38] A. M. Shanshool, M. Bouchakwa, and I. Amous-Ben Amor, "Improved accuracy of pulmonary nodule classification on LIDC-IDRI dataset using deep learning," Procedia Computer Science, Vol. 225, 2023, pp. 394–403.

[39] L. J. Crasta, R. Neema, A. R. Pais, et al., "A novel deep learning architecture for lung cancer detection and diagnosis from computed tomography image analysis," Healthcare Analytics, Vol. 5, 2024, p. 100316.

[40] M. Parola, E. Marcelli, R. del Gratta, R. Guido, F. Vecchio, and M. Vastarella, "Towards explainable oral cancer recognition: Screening on imperfect images via informed deep learning and case-based reasoning," Computerized Medical Imaging and Graphics, Vol. 122, 2024, p. 102433.

[41] R. Ochoa-Ornelas, A. Gudiño-Ochoa, and J. A. García-Rodríguez, "A hybrid deep learning and machine learning approach with Mobile-EfficientNet and Grey Wolf Optimizer for lung and colon cancer histopathology classification," Cancers, vol. 16, no. 22, p. 3791, 2024.

[42] H.-C. Hsieh, C.-Y. Chen, C.-H. Chou, B.-Y. Peng, Y.-C. Sun, T.-W. Lin, Y. Chien, S.-H. Chiou, K.-F. Hung, and H. H.-S. Lu, "Deep learning-based automatic image classification of oral cancer cells acquiring chemoresistance in vitro," PLOS ONE, vol. 19, no. 11, e0310304, 2024.

[43] F. A. Khalid, S. Bashir, M. A. Mustafa, M. Ahmad, I. Ashraf, M. A. Khan, and M. Raza, "An efficient colorectal cancer detection network using atrous and hybrid convolution in colonoscopy images," Scientific Reports, vol. 14, p. 70117, 2024.

[44] M. A. Sharkas and O. Attallah, "Color-CADx: Discrete cosine transform-powered triple convolutional neural networks for colorectal cancer diagnosis," Scientific Reports, vol. 14, p. 70863, 2024.

[45] L. Wang, "Mammography with deep learning for breast cancer detection," Frontiers in Oncology, vol. 14, 1281922, 2024.

[46] M. Hasan, "Deep learning for breast cancer detection: Comparative analysis of ConvNeXT and EfficientNet," arXiv preprint, arXiv:2501.09876, 2025.

[47] M. Ahmadi, N. Karimi, and S. Samavi, "A lightweight deep learning pipeline with DRDA-Net and MobileNet for breast cancer classification," arXiv preprint, arXiv:2403.11135, 2024.

[48] T.-L. Huynh, T.-D. Le, T. V. Nguyen, T.-N. Le, and M.-T. Tran, "Efficient 3D brain tumor segmentation with axial-coronal-sagittal embedding," arXiv preprint, arXiv:2506.00434, 2025.

[49] A. Sadraoui, S. Martin, E. Barbot, A. Laurent-Bellue, J.-C. Pesquet, C. Guettier, and I. Ben Ayed, "A transductive few-shot learning approach for classification of digital histopathological slides from liver cancer," arXiv preprint, arXiv:2311.09821, 2023.

[50] R. Pandian, V. Vedanarayanan, D. N. S. Ravi Kumar, and R. Rajakumar, "Detection and classification of lung cancer using CNN and GoogleNet," Measurement: Sensors, vol. 24, 100588, 2022.